



Changes of tropical cyclone landfalls in South China throughout the twenty-first century

Charlie C. F. Lok¹ · Johnny C. L. Chan¹

Received: 30 June 2017 / Accepted: 20 November 2017 / Published online: 1 December 2017
© Springer-Verlag GmbH Germany, part of Springer Nature 2017

Abstract

The nested regional climate/mesoscale modelling system developed by the authors is applied to the Hadley Centre Global Environment Model version 2-Earth System global model outputs to project future changes of landfalling tropical cyclone (TC) activity in the South China region. Results show that the modelling system is capable of reproducing the current TC landfall climatology, although it exhibits a noticeable southward bias of TC activity in the western North Pacific. Future projections show a continuous northward migration of TC activity in the western North Pacific throughout the twenty-first century. Fewer TCs making landfall in South China are projected in the late century, but these landfalling TCs tend to be more intense. Investigations in the large-scale environment suggest that despite warmer sea surface temperature and weaker vertical wind shear, the drier and less cyclonic lower atmosphere all-season is responsible for the reduced TC activity. However, once a TC is formed, the environment it stays in is as wet as today and so it can intensify further than the present-day TCs. Inter-annual variability is also explored, and the influence of the ENSO variation appears to be smaller.

Keywords Tropical cyclone landfall · Tropical cyclone intensity · Climate projection · Downscaling · Regional climate model · WRF · East Asia

1 Introduction

As tropical cyclones (TCs) pose a significant threat to human society, the question of how TCs will respond to the anthropogenic climate change has become a key research topic. Emanuel (2005) and Webster et al. (2005) examined TC best tracks since the Second World War, and they claimed that TCs have become more intense over the past 50 years. However, others argued that such changes can be attributed to inter-annual and inter-decadal oscillations instead (e.g. Chan 2006; Chan and Xu 2009). Furthermore, while two later studies (Holland and Bruyère 2014; Klotzbach and Landsea 2015) also found an upward trend in the proportion of intense TCs, they both noted a flattening out of the trend in the last ten years. They argued that some of the signals previously reported might be attributed to the improving measurements instead of human-induced warming.

In search of an answer, Knutson et al. (2010) examined numerical model projections and reported that a 6–34% decrease in the number of TCs but a 2–11% increase of TCs intensity globally. Based on 13 models from the fifth phase of the Coupled Model Intercomparison Project data (Taylor et al. 2012, hereafter CMIP5), Tory et al. (2013) also found a global reduction in TC activity with a similar magnitude. However, these studies often exhibited large inter-basin and inter-model variations (Camargo 2013).

To investigate changes of TC activity in the warmer climate, downscaling techniques have been applied either statistically (e.g. Emanuel 2013; Villarini and Vecchi 2012) or dynamically (e.g. Knutson et al. 2013, 2015). While most of these studies suggested that TCs tend to be stronger by the end of twenty-first century, mixed responses were reported in many aspects, e.g. number of TCs and geographical distributions.

Efforts have been made in identifying future changes in individual basins. Zhang et al. (2017) downscaled four CMIP5 global models and reported an increase in the number of TCs as well as their intensity in the North Pacific. More importantly, they also identified such changes can be attributed to smaller vertical wind shear and an increase in

✉ Charlie C. F. Lok
Charlie.Lok@my.cityu.edu.hk

¹ School of Energy and Environment, City University of Hong Kong, 83 Tat Chee Avenue, Kowloon Tong, Hong Kong

sea surface temperature. Park et al. (2017) investigated the response in the western North Pacific (WNP) by statistical downscaling and found a northward migration of TC activity by the end of the century. These studies paved the way for further investigation on the regional changes of TC activity.

Based on our ongoing development in seasonal prediction of TC activity in the WNP (e.g. Au-Yeung and Chan 2012; Huang and Chan 2014; Lok and Chan 2017), it is now possible to apply the developed model to project future climate changes. The primary objectives of this study are therefore (a) to investigate future changes of TC activity, in particular variations in TC landfalls in the southern China coast, and (b) to identify possible causes of the changes.

The numerical model and the data used in this study are described in Sect. 2. Model results are presented in Sects. 3 and 4 for the present-day simulation and future climate projection respectively. The results are further discussed and summarised in Sect. 5.

2 Methodology

Future climate projection of TCs making landfall is conducted by dynamical downscaling from a global climate projection model. The modelling system consisting of a regional climate model and a mesoscale model developed by Lok and Chan (2017) is used to simulate the large-scale environment and individual TC intensity. The modelling system and the data used are summarised in this section.

2.1 CMIP5 model data

It is preferable to apply the modelling system to all available CMIP5 global models so that a multi-model ensemble projection can be produced. Unfortunately, our computational power does not have such capacity. Instead, in this study, the modelling system is driven from one of the CMIP5 models. The result of this study, nevertheless, can serve as an example of how such projections can be made so that if computer resources are available, the reader can perform multi-model ensemble estimates. The approach here can also be adopted for projecting landfalling TC activity in other regions.

McSweeney et al. (2015) assessed most of the CMIP5 models extensively and identified some unrealistic models (e.g. they reported that the summer monsoon flow in MIROC-ESM never reaches the Indochina peninsula). We have also examined the 20 CMIP5 models that contain the variables required by the modelling system and publicly available. As Lok and Chan (2017) found that the subtropical ridge is crucial for simulating TC activity in the South

China coast, these model output are compared against the CFSR dataset based on the 500-hPa height over the WNP. Since we are only able to pick one of the models, it is preferable that the selected model is “representative” (i.e. close to the multi-model mean) while at the same time it does not have significant deviation from the present-day climatology. Based on these criteria, we found that the Hadley Centre Global Environment Model version 2-Earth System (Collins et al. 2011, hereafter HadGEM2-ES) is both “representative” and contains a reasonable current climate. Also, HadGEM2-ES is reported as capable of representing the current ENSO variability (Yun et al. 2016; Chen et al. 2017a) as well as TC activity (Camargo 2013; Tory et al. 2014). Therefore, HadGEM2-ES is chosen to be down-scaled in this study.

In order to investigate future changes of TC activity and landfall in the southern China region, two sets of experiments are taken from the HadGEM2-ES model output in this study. The historical experiment is used to evaluate the modelling system in recreating the current climate. The representative concentration pathways 8.5 (RCP8.5) experiment, in which the radiative forcing reaches 8.5 W m^{-2} by the end of this century, is used for future climate projection. The RCP8.5 experiment is the highest emission scenario, and it is selected to estimate the potential response of TC activity to maximum warming. The modelling system is applied to the HadGEM2-ES outputs over four different decades: 1996–2005 from the historical experiment (present-day) and 2030–2039 (2030s), 2060–2069 (2060s) and 2090–2099 (2090s) from the RCP8.5 experiment so that changes throughout the century can be investigated.

2.2 RegCM3-WRF modelling system

The RegCM3-WRF modelling system developed by Lok and Chan (2017) is used to simulate TCs making landfall in Guangdong and Hainan provinces of China (hereafter South China) throughout the twenty-first century. The ICTP Regional Climate Model version 3 (Pal et al. 2007, RegCM3) first simulates the WNP summertime atmospheric circulations. It is a sigma coordinate and compressible model, based on the hydrostatic dynamical core of the fifth-generation Pennsylvania State University-National Center for Atmospheric Research Mesoscale Model. The same physical packages are chosen following previous studies of our group (Au-Yeung and Chan 2012; Huang and Chan 2014; Lok and Chan 2017): the modified Biosphere-Atmosphere Transfer Scheme for the land surface processes (Dickinson et al. 1986), the boundary layer scheme of Holtslag et al. (1990), the radiative transfer scheme of the NCAR Community Climate Model version 3 (Kiehl

et al. 1996), Pal et al. (2000)'s subgrid explicit moisture scheme for resolvable non-convective precipitation, and the Chow et al. (2006) modified MIT scheme for cumulus convection (Emanuel and Živković Rothman 1999). Chow et al. (2006)'s modification prevents unrealistic model convective precipitation, and the following large-scale criteria must be met in order to precipitate numerically: relative humidity must be at least 55%, and the low-level relative vorticity must be greater (smaller) than $-(+)\text{12} \times 10^{-6} \text{ s}^{-1}$ in Northern (Southern) Hemisphere.

RegCM3 takes the HadGEM2-ES global model output as the boundary conditions every 6 h using a 15-grid buffer relaxation method, and the sea surface temperature from HadGEM2-ES is fed into RegCM3 every week. There are 18 vertical levels from the surface to 1 hPa, with the horizontal resolution of 50 km. The model domain covers from 90°E to 170°W and 15°S to 45°N . For every TC season, RegCM3 starts in early April and runs until the end of October. A total of 8 member ensemble simulations are performed to address model uncertainty. Each ensemble member has its own model initial time and is separated by 6 h. The first ensemble member starts at 1 April 00Z and the last member is at 2 April 18Z. Analyses are based on the output between May and October, as the first simulated month is regarded as the spin-up period.

The same TC tracker developed in previous studies (Au-Yeung and Chan 2012; Huang and Chan 2014; Lok and Chan 2017) is used to identify TC-like vortices from the RegCM3 model outputs. The tracker locates all local 850-hPa vorticity maxima every 10° latitude square box. A vortex is considered as a TC if the following criteria are satisfied: (a) the magnitude of the vorticity patch is greater than $450 \times 10^{-6} \text{ s}^{-1}$; (b) 300-hPa air temperature at the vortex centre is 1 K warmer than the average of a 15° latitude square box from the vortex centre; (c) the vortex has met criteria (a) and (b) for at least 48 h consecutively; and (d) the genesis position is over the ocean.

We trace all these TC-like vortices from the RegCM3 simulation, and identify TCs which make landfall in South China (defined as the TC centre is within 100 km from the coastline). The Weather Research and Forecast model version 3.7 (hereafter WRF) is then applied to the RegCM3 output to obtain detailed structure and intensity of all these landfalling TCs. The configuration of the WRF model is the same as Lok and Chan (2017), and it is briefly summarised in the following paragraphs.

The WRF model contains two domains of 151×151 (outer) and 181×181 grid points (inner). The horizontal resolution of the outer (inner) domain is 27 km (9 km). The model starts at 60 h prior to the RegCM3 TC landfall time so that the TC has enough time to spin up. The outer domain is fixed at the RegCM TC position 30 h before landfall. A

vortex tracing algorithm based on 500-hPa relative vorticity is used to keep the TC within the inner domain. As such, the inner domain is relocated to the WRF TC centre every 15 min. There are 28 vertical levels from the surface up to 100 hPa, and the timestep ratio of the outer and inner domain is 1:3.

The following physical packages are used in accordance to the sensitivity test results documented in Lok and Chan (2017): the Ferrier et al. (2002) schemes for microphysics, the Yonsei University scheme (Hong et al. 2006) for the planetary boundary layer, the Kain (2004) scheme for cumulus convection, the Rapid Radiative Transfer Model (Mlawer et al. 1997) for radiation and the MM5 similarity scheme based on Monin and Obukhov (1954) for the surface layer. The land surface model is a 5-layer thermal diffusion model since RegCM3 has no soil temperature output.

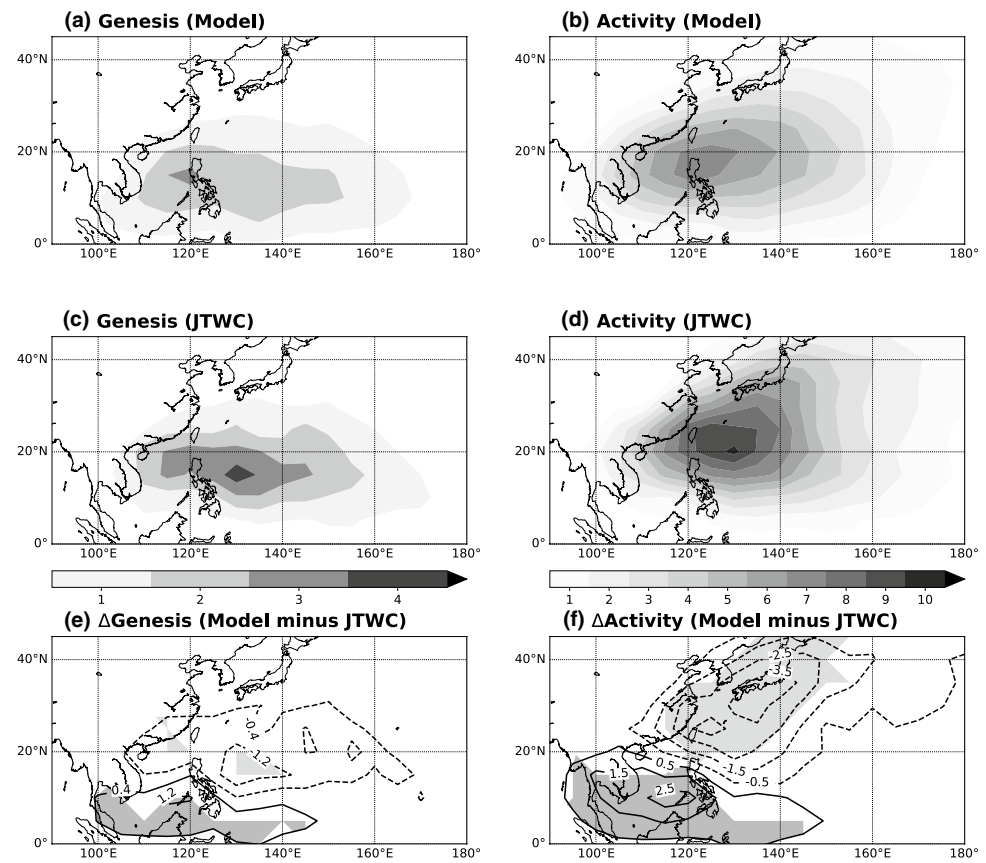
3 Present-day TC climatology

It is important to identify systematic biases of the modelling system, and so in this section the simulated and observed present-day TC climatology are compared. The present-day climatology is reproduced by running the RegCM-WRF modelling system based on the historical experiment of the HadGEM2-ES global model output for 1996–2005. Actual TC tracks and large-scale circulations during the same period are obtained from the Joint Typhoon Warning Center (JTWC) best track dataset (Chu et al. 2002) and the NCEP Climate Forecast System reanalysis data (CFSR, Saha et al. 2010) respectively.

The modelling system is found to produce fewer TCs than the observed (Fig. 1). The ensemble mean number of TCs between May and October is 16.6 per year, which is 81% of the actual number of TCs reaching 34 knots or above (20.4), and the difference is significant at the 99% confidence level. Apart from the reduced number, genesis location and tracks are also different. Simulated TCs most likely form to the west the Philippines, while in the real world the maximum is located near 130°E . Consequently, more TCs enter the South China Sea, but fewer TCs move poleward to Japan in the model (Fig. 1f). A similar southward bias was also reported in our previous study (Lok and Chan 2017).

Biases in the simulated TC activity can be explained by the difference in the large-scale environment between the model and the reanalysis. The model has a stronger 850-hPa southwesterlies than the observed (Fig. 2f). As the outbreak of the southwest summer monsoon is often considered to be favourable for cyclonegenesis in the South China Sea (Chen et al. 2017b), overestimation of the southwesterly flow leads to a stronger cyclonic flow

Fig. 1 May–October TC genesis density (**a**, **c**) and track density (**b**, **d**) for the RegCM3 ensemble simulations (**a**, **b**) and JTWC best track (**c**, **d**) over the period from 1996 to 2005. **e** Differences in genesis density between the modelling system and observation [(**a**) minus (**c**)]. Positive (negative) differences which are significant at 95% confidence level are shaded in dark (light) grey. **f** As (**e**) but for the differences in track density [(**b**) minus (**d**)]. Genesis (track) density is defined as the number of TC formation (passage) per $5^\circ \times 5^\circ$ square per year



and low-level convergence in the South China Sea in the model present climate. Subsequently the model generates more TC activity in the South China Sea than the observed. A recent study conducted by Liang et al. (2017) also noted a similar overestimation of the southwest monsoon in the HadGEM2-ES model, and the bias propagated into the large-scale environment of their downscaled simulation as well. In fact, we also identify similar biases in the large-scale environment from original HadGEM2-ES historical experiment (not shown).

On the other hand, the simulated subtropical high is located further south than the actual (Fig. 2a, c), suppressing TC genesis east of the Philippines. The displacement of the subtropical ridge also leads to westerlies flow prevailing at 20°N at 500-hPa instead of easterlies. As a result, a significant negative bias in the TC activity to the north of 20°N latitude (Fig. 1f) is found.

As the total number of TCs is reduced along the East Asia coast, the modelling system also underestimates the number of landfalls in South China (2.3 verse 3.0, but significant only at 90% confidence level). Nevertheless, the simulated seasonal variations in both the number of landfalls and TC intensities at landfall are similar to the present-day climate (Fig. 3). In particular, the probability

density functions of the simulated and observed TC intensities at landfall match each other very closely, having 87% area in common. The annual power dissipation index (Liu and Chan 2017a, hereafter APDI, which is the sum of cubes of all TC maximum sustained wind speed at landfall in South China) to summarise seasonal TC landfall activity. As the index is a function of the number of TCs and their intensity, the modelling system underestimates the index by 3×10^5 knots³. However, this underestimation is statistically insignificant, as the p value reaches 0.24. Also, the observed APDI distribution stays within the simulated envelope as well (not shown). The result highlights the modelling system's ability in simulating TCs making landfall in the South China coast.

Since only one CMIP5 global model is applied in this study, it is not surprising that the simulation contains some systematic deficiencies. Nevertheless, the above analyses indicate that the modelling system can still reasonably re-create the present-day climatology. When the modelling system is applied to the future climate change scenarios, we will compare the result with this simulated climatology to minimise the influence of systematic biases.

Fig. 2 Seasonal (May–October) mean flow pattern at 500-hPa (a, c) and 850-hPa (b, d) from RegCM3 (a, b) and CFSR (c, d) for the period of 1996 and 2005. Wind speeds (m s^{-1}) are shaded. e Differences of 500-hPa flow patterns between the model and observation [(a) minus (c)]. Significant differences in the wind fields at the 95% confidence level are shaded. f As (e) but for 850-hPa [(b) minus (d)]

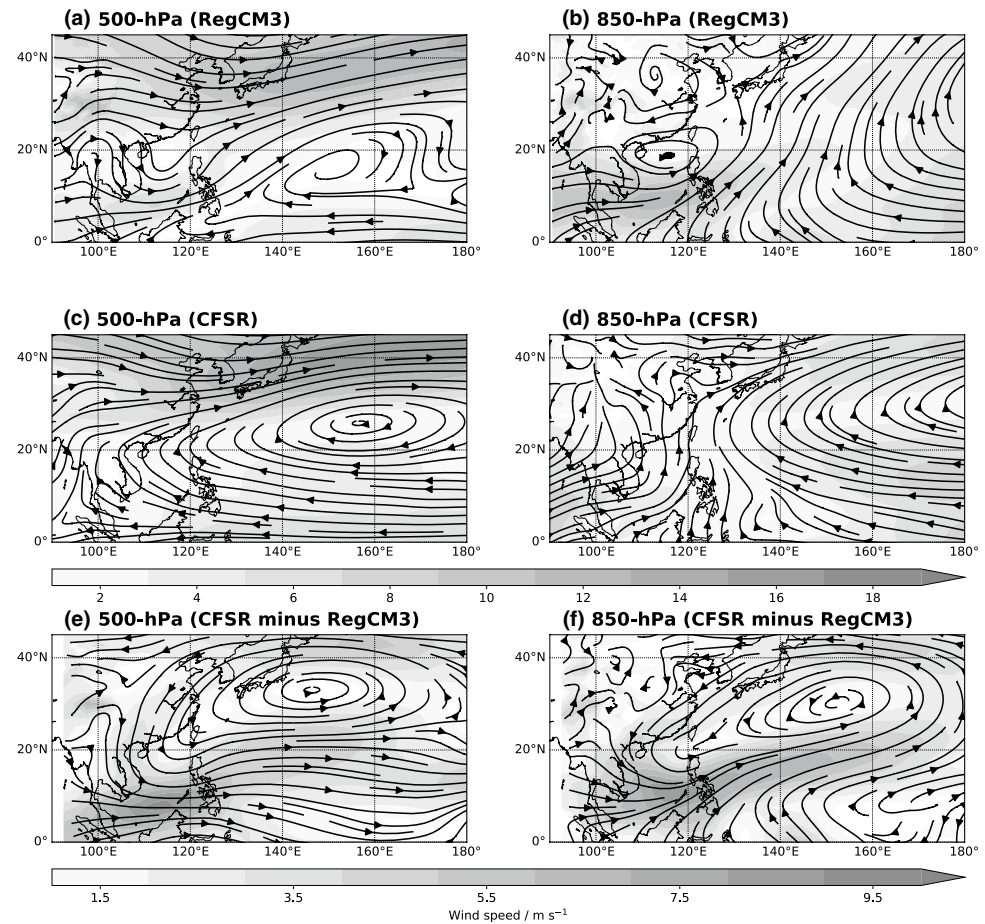
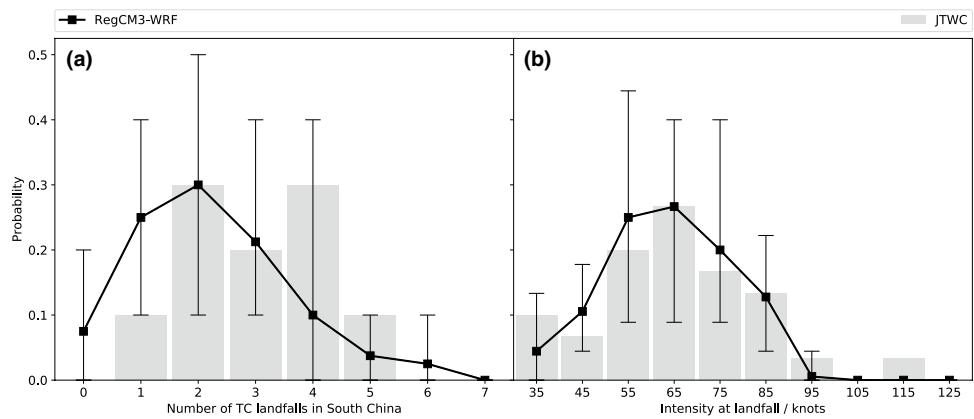


Fig. 3 Probability density functions of a number of TC landfalls between May and October in South China and b TC maximum sustained wind at the time of landfall in South China. Grey bars are the JTWC best track, and squared lines represent the RegCM3-WRF modelling systems simulation with whiskers showing the spreads between ensemble members



4 Twenty-first century climate projection

In this section, the modelling system is applied to the RCP8.5 experiment of the HadGEM2-ES model to project the twenty-first century TC climatology. The modelling

system is run for 10 years every three decades (2030s, 2060s and 2090s). The simulation results are compared with the “present-day” run to analyse future changes.

Table 1 Statistics of TC activity from the RegCM3-WRF modelling system projection

Variables	1996–2005	2030s	2060s	2090s
Number of TC	16.6	15.1	16.7	12.8
Change from the present climate		-1.6	0.0	-3.8
Mean latitude of TC genesis	13.6	14.4	15.4	17.2
Change from the present climate		0.8	1.7	3.5
Mean longitude of TC genesis	133.0	132.9	135.0	134.5
Change from the present climate		-0.1	1.9	1.4
Number of landfalls in South China	2.2	1.7	1.7	1.5
Change from the present climate		-0.5	-0.5	-0.8
APDI of South China (10^5 knots 3)	6.9	5.7	6.6	6.8
Change from the present climate		-1.2	-0.3	-0.1

10-year ensemble means of the variables are shown for all decades. Significant changes (95% confidence level) are highlighted by bold-face

4.1 Changes in TC activity

In general, the modelling system projects a decrease in the annual number of TCs in the WNP (Table 1). A 23% reduction by the end of this century is projected, which

is consistent with some previous CMIP5 studies [e.g. Tory et al. (2013) reporting up to 30% decrease from the selected CMIP5 global models, and Knutson et al. (2015) projecting 35% fewer TCs from the downscaling of CMIP5]. However, the response of TC activity to the warmer climate scenario varies across the four simulated decades (Fig. 4a). The reduction is observed in the first and the last thirty years of this century, whereas in 2060s the number of TCs is about the same as today. Nevertheless, the number of TCs projected in 2090s is the lowest of this century. It may indicate a combined effect of inter-decadal variation and global warming on TC activity, which a continuous simulation throughout the century is needed to further investigate.

Apart from the reduction of TC activity, the projected locations of TC genesis and tracks are also different from the present-day climatology. A noticeable northward shift is found from both the TC genesis positions (Fig. 5) and TC activity (Fig. 6). The mean latitude of TC genesis gradually moves from 13.6°N of the present-day to 17.2°N in the 2090s. For the track patterns, in both the 2030s and the 2090s when fewer TCs are formed than the previous thirty years, TC frequency significantly reduces to the south of 20°N (Fig. 6b, g), and in the 2060s (increased number of TCs), more TCs enter the northern part of the domain (Fig. 6d).

Fig. 4 Statistics of 10-year ensemble means of **a** the total number of TCs in the WNP, **b** the number of TCs making landfall in South China and **c** the APDI (10^5 knots 3) of South China. Whiskers show the 95% confidence intervals of the variables

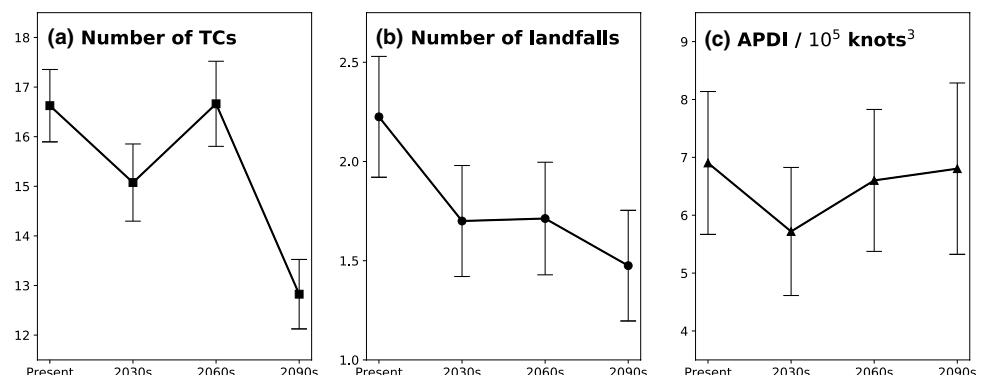
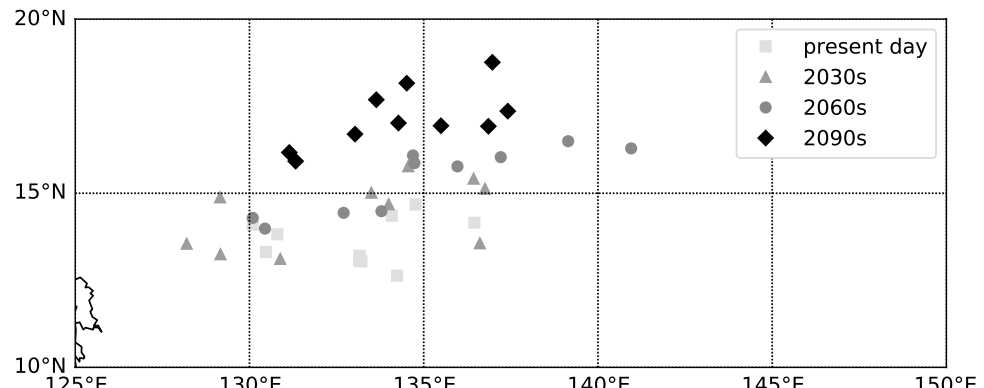


Fig. 5 Seasonal mean positions of TC genesis projected by RegCM3. Light grey squares represent the period between 1996 and 2005, grey triangles for the decade of 2030s, dark grey circles for the decade of 2060s, and black diamonds for the decade of 2090s



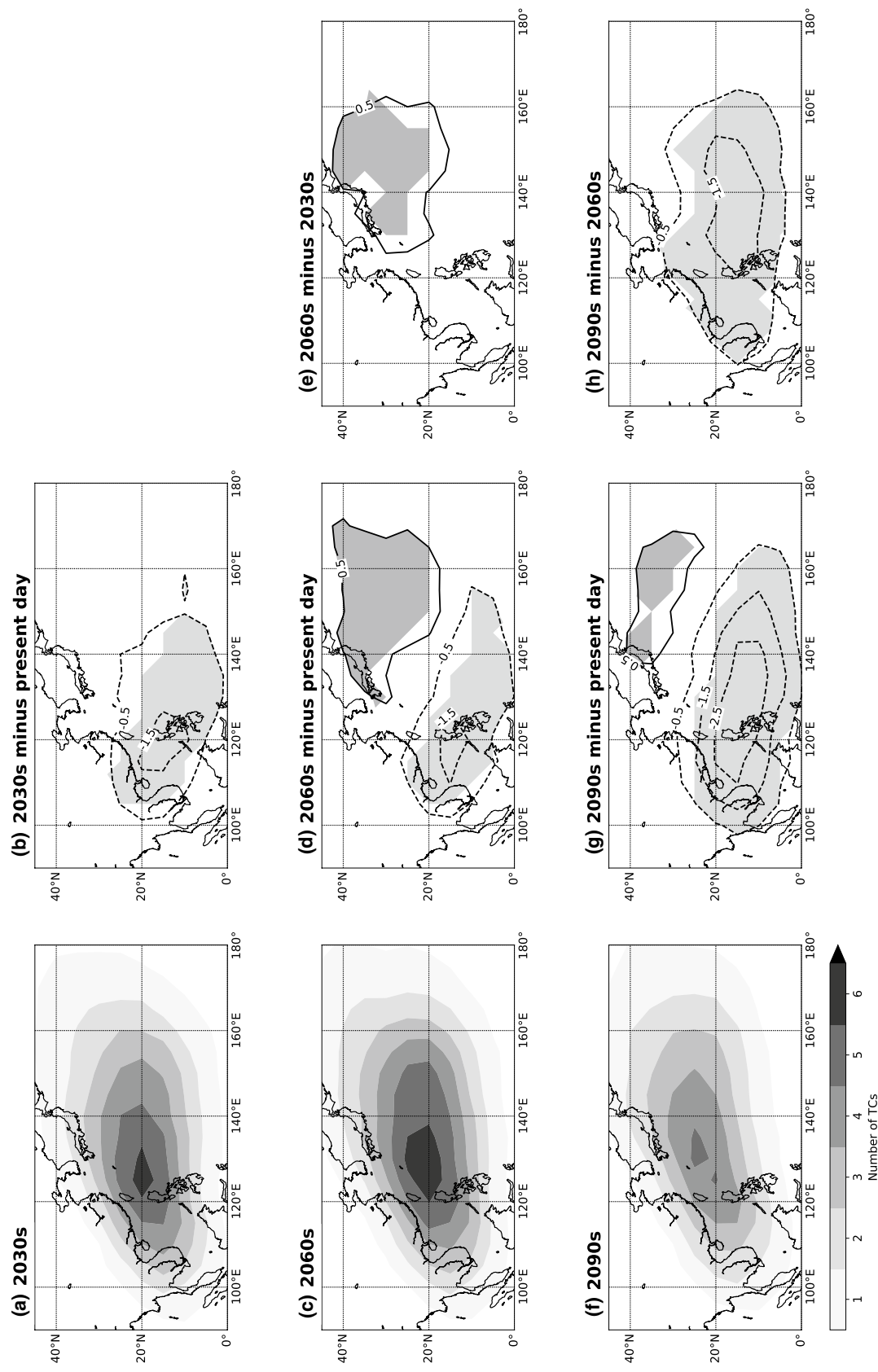
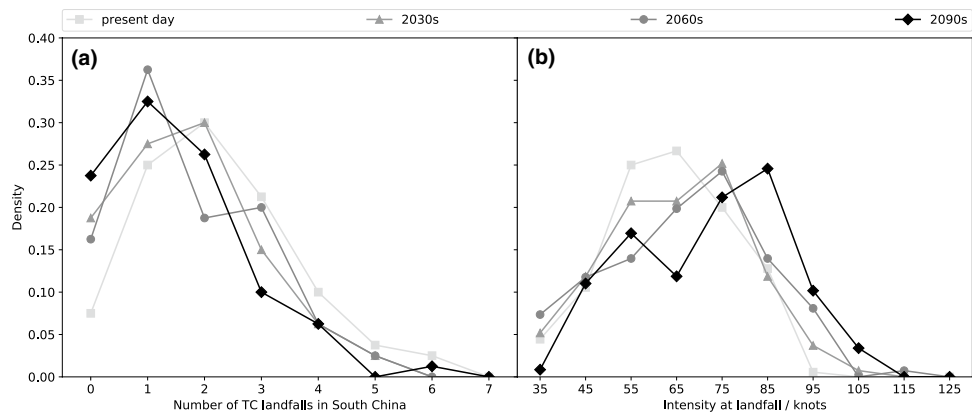


Fig. 6 May–October TC track densities projected by RegCM3 of the decades of **a** 2030s, **c** 2060s and **f** 2090s. Projected changes in track density from the present-day to **b** 2030s, **d** the 2060s and **g** the 2090s. **e**, **h** Same as **(d)** and **(g)** but changes to previous 30 years. Positive (negative) changes significant at 95% confidence level are shaded in dark (light) grey. Track density is defined as the number of TC passage per $5^\circ \times 5^\circ$ square per year

Fig. 7 Probability density functions of **a** number of TC landfalls between May and October in South China, **b** TC maximum sustained wind speeds (knots) at the time of landfall in South China. Light grey squared dashed lines are the period between 1996 and 2005, grey lines with triangles are the 2030s, dark grey circled dashed lines are the 2060s and black lines with diamonds are the 2090s



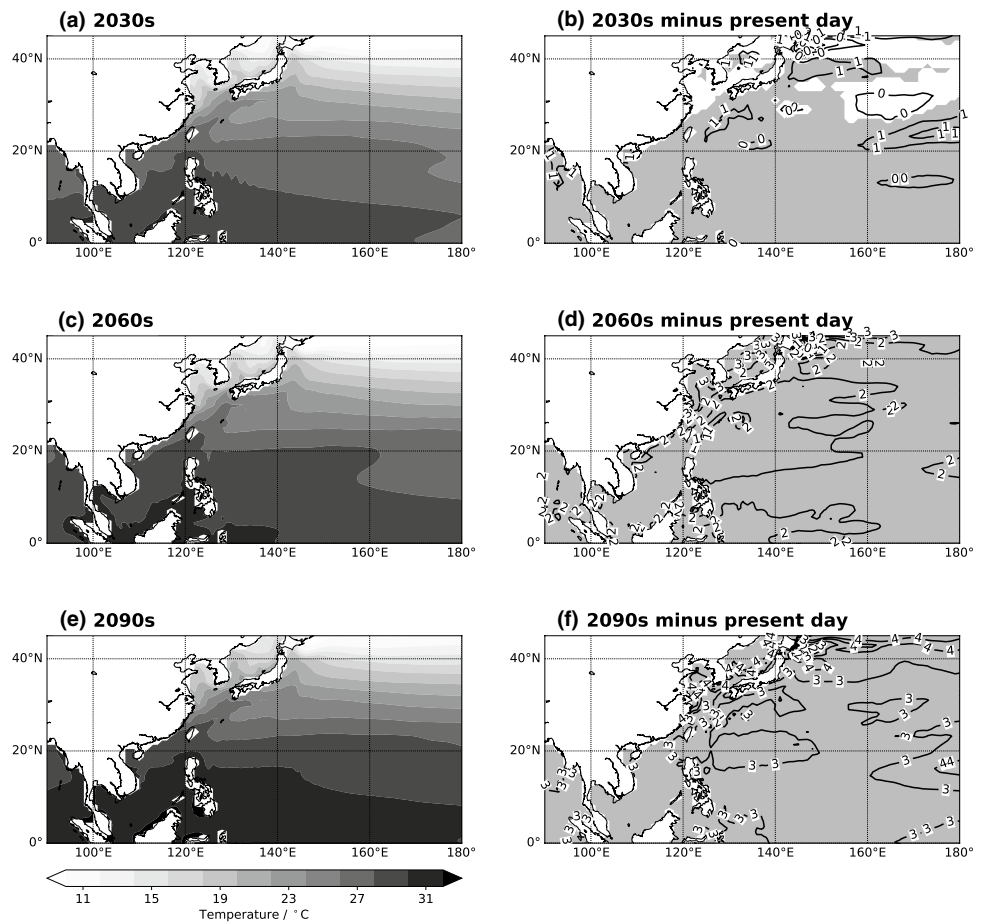
Such persistent northward shift projected by the modelling system is consistent with the analysis of Park et al. (2017) who obtained an increase of TC occurrence in northeast Asia by the end of the century.

Following these changes in the projected TC activity, the number of TCs making landfall in South China significantly drops from 2.3 of the present-day simulation to 1.5 in the late twenty-first century. Seasonally, the likelihood of less

than 2 TCs making landfall per year jumps from 30 to 55% by the end of the century, and only 1 of 80 seasonal ensemble simulations has more than 4 TCs making landfall in the region in the 2090s (Fig. 7a).

In terms of TC intensity, Fig. 7b suggests that TCs tend to be more intense when they make landfall by the late twenty-first century. The peak of the intensity distribution shifts from 65 knots of the current climate to 85 knots at the end

Fig. 8 Averaged May–October SST ($^{\circ}$ C) projected by RegCM3 for the decades of **a** 2030s, **c** 2060s and **e** 2090s. Projected changes in track density from present-day to **b** the 2030s, **d** the 2060s and **f** the 2090s. Positive (negative) changes significant at 95% confidence level are shaded in dark (light) grey



of the century. In fact, the peak intensity of the simulated TC are stronger in the warmer climate, in agreement with previous reports (e.g. Zhang et al. 2017; Ying et al. 2012, both identified an increase in TC intensity). Balancing the increased probability of intense TCs and the reduction of TC landfalls, no significant change in the APDI throughout the century is found. Also, the PDF of APDI are very similar in all four decades (not shown).

4.2 Changes in the large-scale environment

Changes in the future TC landfall activity can be attributed to the large-scale environment. Since the highest emission scenario of CMIP5 is used to drive the modelling system in this study, the underlying SST from the source model is undoubtedly increasing throughout the century (Fig. 8). As warm ocean is seen as a favourable condition for TCs (e.g. Emanuel 1986; Shay et al. 2000), the continuous warming in the projected ocean can enhance TC energetics by the end of this century.

Furthermore, vertical wind shear between 200- and 850-hPa in the future climate is weaker than the present-day. A

robust basin-wide reduction in the seasonal mean magnitude of the vertical wind shear is found (not shown). More importantly, there is also a continuous increase in the number of weak shear days (Fig. 9), defined as the magnitude of the vertical wind shear less than 10 m s^{-1} . Strong shear events are less likely to occur in the future, especially in the low latitudes where the number of weak shear days increases by two weeks per thirty years. Since strong shear is considered as an inhibitor to TC development (Black et al. 2002), weaker vertical wind shear by the end of the twenty-first century is also a positive change for TCs.

The projected changes in the SST as well as the vertical wind shear appear to be the reasons of more intense TCs in the 2090s than the present-day, as they are often regarded as the controls of TC intensity (e.g. Emanuel 1999; Emanuel et al. 2004). However, the number of TCs in the future climate is projected to decrease, opposite to the changes in their intensities and contradicting to Zhang et al. (2017) who reported increasing trends instead. Some other factors must be responsible for prohibiting TC formation in the future, and so the projected low-level

Fig. 9 Same as Fig. 8, but for the number of days which vertical wind shear between 200- and 850-hPa weaker than 10 m s^{-1}

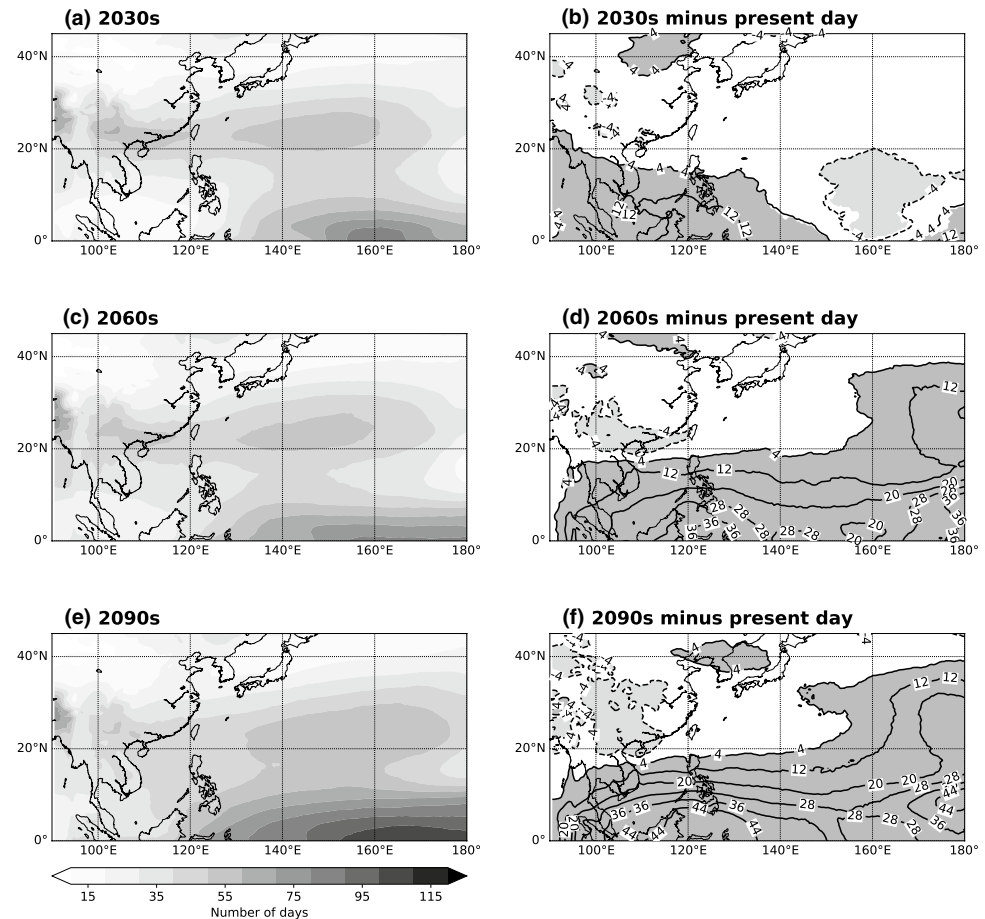
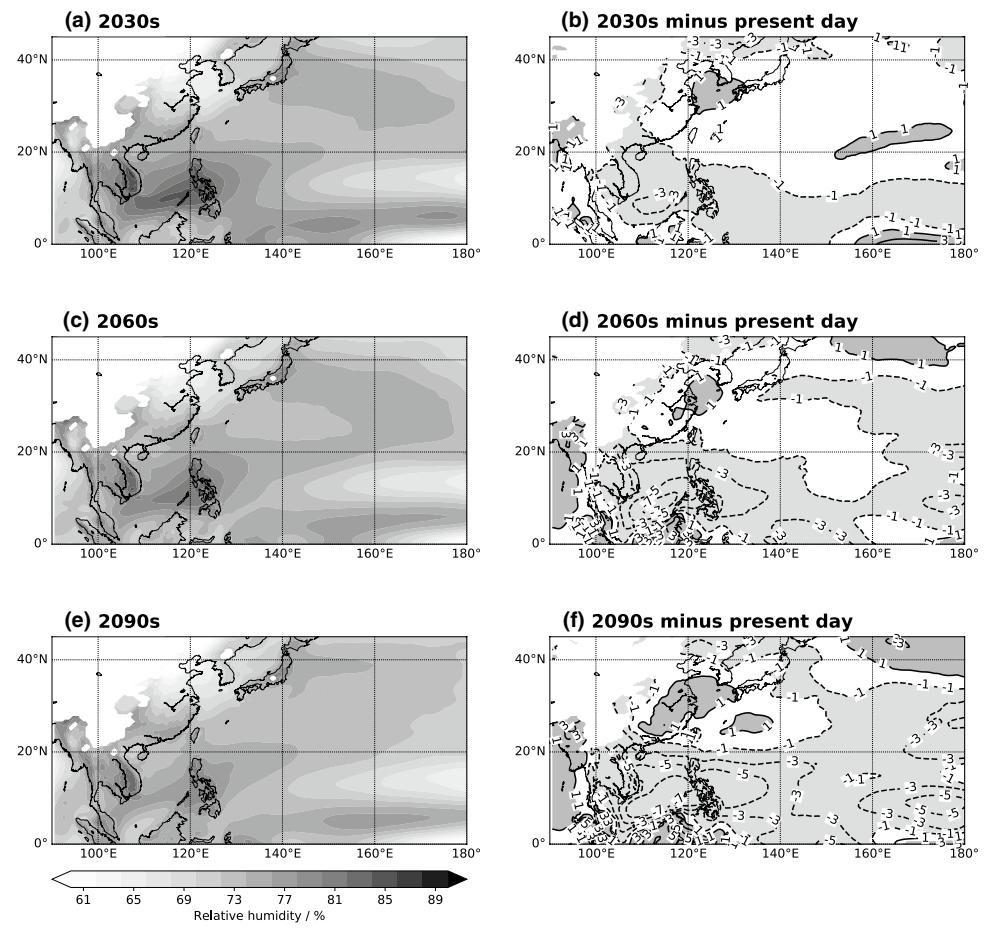


Fig. 10 Same as Fig. 8, but for the 850-hPa relative humidity (%)



atmosphere in the warmer world is discussed in the following paragraphs.

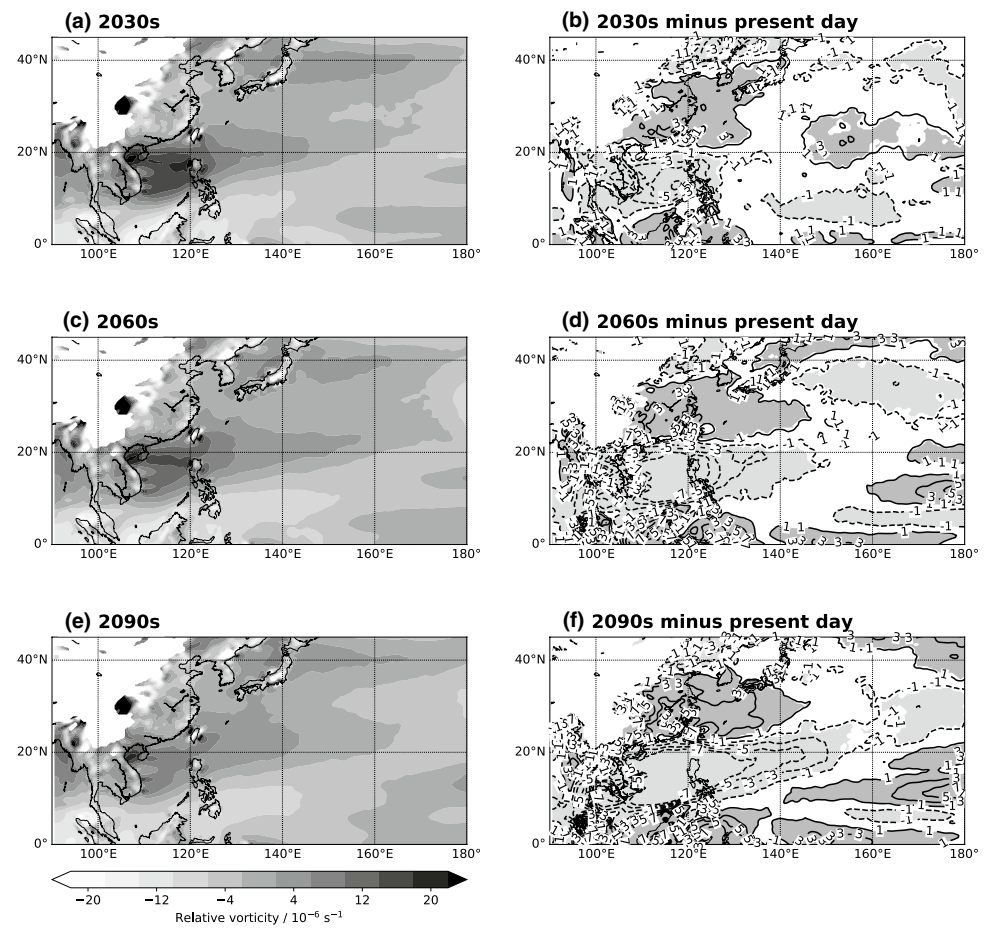
Low-level relative humidity is expected to be lower consistently to the south of 20°N throughout the century (Fig. 10). On the other hand, it becomes wetter in the East China Sea and Yellow Sea by the 2090s. Similar changes in low-level vorticity are also projected: the area of cyclonic vorticity in the South China Sea expands further north but the magnitude significantly weakens (Fig. 11). These changes of the two variables lead to less (more) favourable environment around 15°N (30°N) for TC. As many studies (e.g. McBride and Zehr 1981; Kerns and Chen 2013; Yoshida et al. 2017) have pointed out, a low-level convective vortex is a necessary condition of TC development. Reducing the low-level humidity and cyclonic vorticity can represent fewer pre-TC disturbances, and so fewer TCs are projected. The patterns of the projected changes are consistent with the northward migration of TC activity.

Since there are two competing environmental forcings on the future TC activity, it is necessary to further diagnose

their net effect on TCs. Here, the genesis potential index (Emanuel and Nolan 2004, hereafter GPI) is used to analyse the total environmental forcing on the TC formation, as demonstrated by a number of studies (such as Camargo et al. 2007; Murakami and Wang 2010). The index can be regarded as a large-scale indicator of potential TC formation, and it is defined as $\text{GPI} = |10^5 \eta|^{1/2} \left(\frac{\text{RH}}{50} \right)^3 \left(\frac{V_{\text{pot}}}{70} \right)^3 (1 + 0.1 \text{VWS})^{-2}$, where η is 850-hPa absolute vorticity in s^{-1} , RH is 600-hPa relative humidity in percentage, V_{pot} is potential intensity in m s^{-1} , and VWS is vertical wind shear between 200- and 850-hPa in m s^{-1} . Potential intensity is the maximum intensity a TC may reach given the atmospheric instability and SST (Bister and Emanuel 1998, 2002), and the calculation code is obtained from <http://emanuel.mit.edu/products> (last accessed on 1 Sept 2017).

Figure 12 illustrates how the total environmental forcing on TC changes throughout the twenty-first century. The index increases mostly in the northern part of the domain, and it reduces significantly in the South China Sea. These

Fig. 11 Same as Fig. 8, but for 850-hPa relative vorticity (10^{-6} s^{-1})



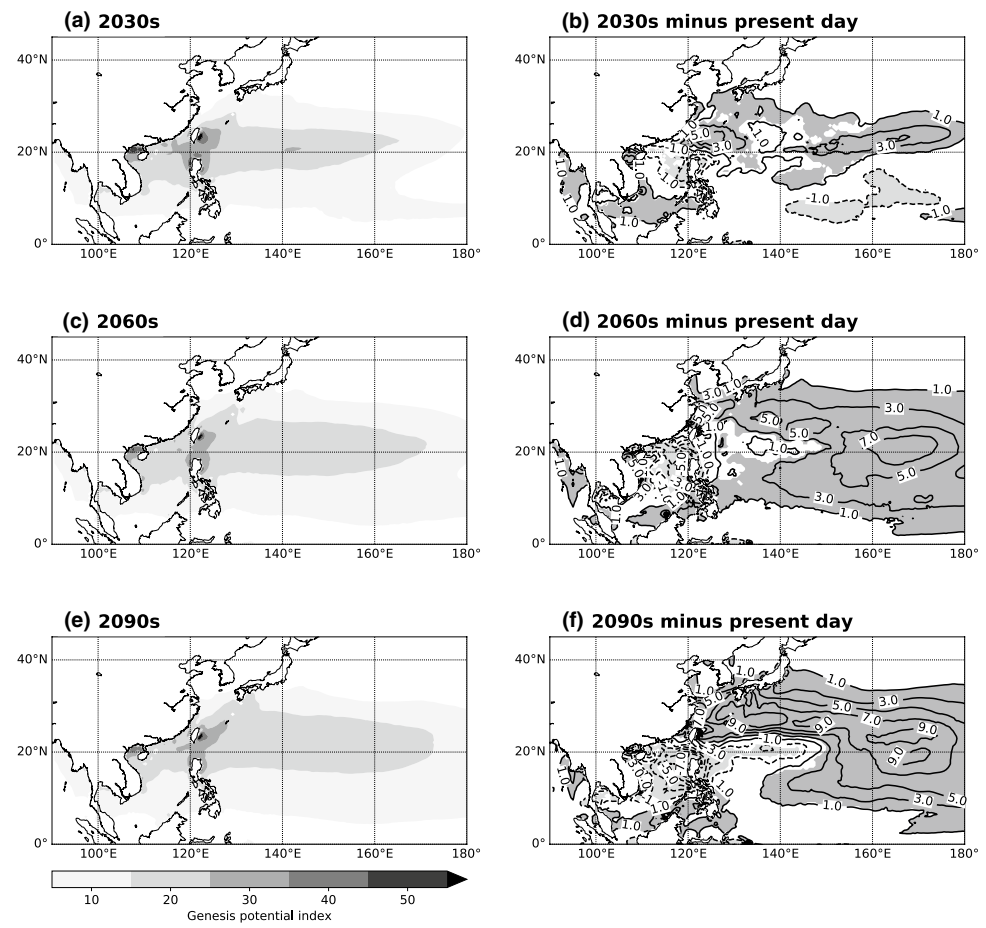
changes are consistent with the seen northward shift in the TC genesis as well as the frequency (Fig. 6). As the projected changes in the low-level humidity and vorticity also show similar patterns as the GPI, it can be said that these two variables outweigh the shear or SST in terms of TC genesis in the future climate.

The large-scale circulation is also responsible for the reduced TC landfall activity in South China in the late twenty-first century. Figure 13 shows the evolution of seasonally-averaged 850–200 hPa layer mean circulation throughout this century. In general, there are stronger than present-day westerlies in the northern South China Sea and an enhanced cyclonic flow over the East China Sea, preventing TCs entering the South China Sea. Lok and Chan (2017) pointed out that such a flow pattern anomaly is related to the reduction of TC landfalls in South China. Since a significant reduction of the number of TC landfalls is also projected, the result reaffirms the previous finding. Also as seen in Fig. 11, the flow in the South China Sea becomes more anticyclonic (Fig. 13b, d, f), leading to fewer TCs make landfall in the region by the end of the twenty-first century.

While the projected seasonal means of the large-scale environment can explain the decreasing number of TCs in the WNP and the number of landfall in South China, in terms of the TC, intensity the environment during active TCs can be more important than the seasonal means. Therefore, composites of the projected changes in the low-level relative humidity and vertical wind shear have been made to highlight the large-scale influence on the TC intensity (Fig. 14).

The vertical wind shear is still generally weaker in the future, especially in the South China Sea (Fig. 14a, c, e). On the other hand, while the seasonal relative humidity in the tropics is projected to be lower by the end of the century, during TC passages the low-level atmosphere does not become drier in the same magnitude. Figure 14b, d, e show that the relative humidity in the northern South China Sea in the projected future climate is about the same as the present-day when TCs are embedded in the atmosphere. Given the warmer underlying SST in the future (Fig. 8), if a TC manages to form in the future, it will experience a more favourable environment and consequently tend to be more intense than today.

Fig. 12 Same as Fig. 8, but for the genesis potential index



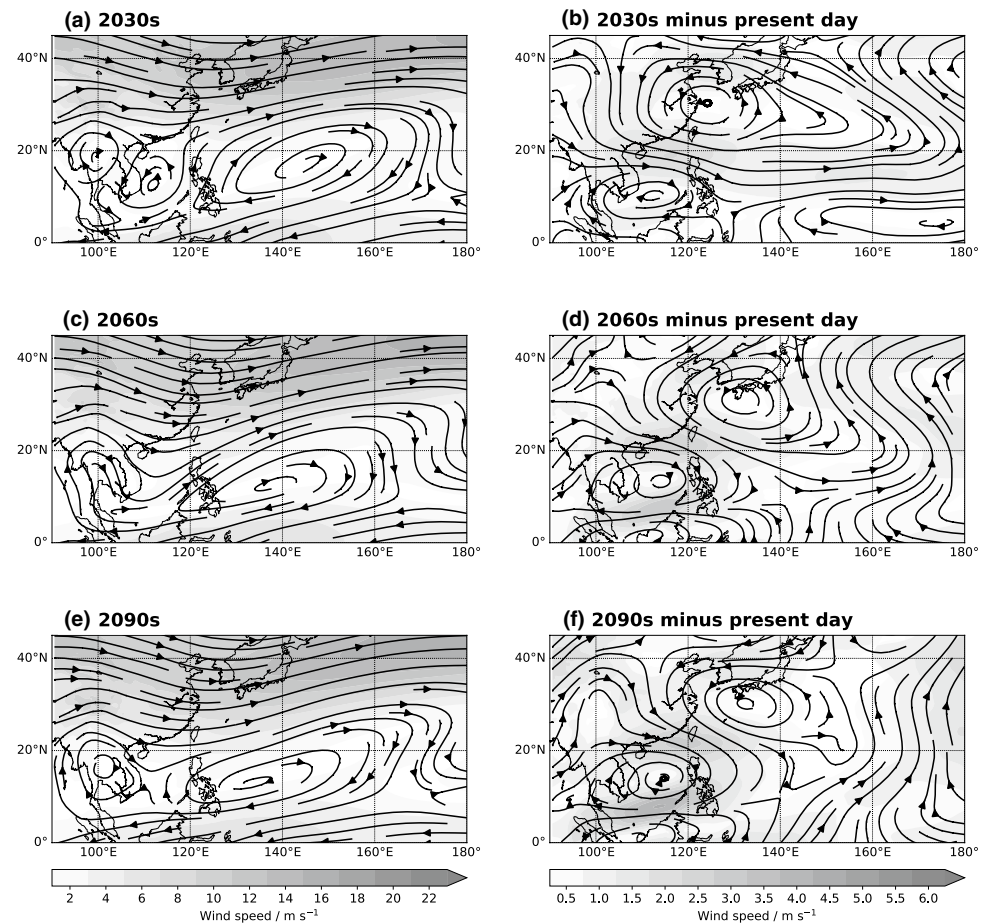
The above analyses in the large-scale environment provide the reasons of projected changes in TC landfall activity. In general, the area of cyclonic vorticity is projected to expand further north, but the magnitude is weaker. Alongside with the drier low-latitudes, fewer TC genesis is projected, and if TCs form they tend to be further north. The mean flow pattern in the South China Sea is projected to more anticyclonic, with enhanced-westerlies at 20°N, leading to fewer TCs entering the South China Sea from the open WNP and less TC landfalls in South China. On the other hand, once TCs are formed, weaker vertical wind shear, as well as more moisture contributed by a warmer ocean with the same of low-level relative humidity in a warmer world make them easier to intensify, and thus more intense TCs making landfall are projected. It should be noted that while there are some signals of inter-decadal variability in the WNP TC activity throughout this century (e.g. the number of TCs), changes in the projected large-scale environment are mostly relative to the present-day climate. Since a “snapshot” approach is used in this study (i.e. simulations are performed every thirty years), there might not be enough

simulations to analyses the inter-decadal variability in TC activity.

5 Discussions and conclusions

In this study, the RegCM3-WRF modelling system is applied to the HadGEM2-ES model to produce projection of the twenty-first century. It is found that HadGEM2-ES overestimates the low-level southwesterlies in the present-day simulation, and the bias remains in the RegCM3 simulated atmosphere. Nevertheless, the modelling system is still capable of reproducing a reasonable TC landfall activity in South China. Under the highest emission scenario RCP8.5, the model projects fewer TCs make landfall in South China by the late twenty-first century. However, these TCs are projected to be more intense at landfall, and APDI of South China remains unchanged. There is a robust reduction in the number of TC in the WNP, and a significant northward migration is observed.

Fig. 13 RegCM3 projected seasonal average of 850–200 hPa layer-mean flow patterns for the decades of **a** 2030s, **c** 2060s and **e** 2090s. Projected changes in the layer-mean flow pattern from the present-day to **b** the 2030s, **d** the 2060s and **f** the 2090s. Significant differences in the wind fields at the 95% confidence level are shaded



It is found that the tropical WNP is getting drier with weaker cyclonic vorticity, which is responsible for the reduction of TC activity. Furthermore, the development of an anti-cyclonic flow in the northern SCS throughout the century results in fewer TCs entering the region. On the other hand, the warmer ocean and weaker vertical wind shear contribute to the projection of more intense TCs in the late twenty-first century.

We find a similar correlation between the 500-hPa geopotential high and the TC landfalls in South China (Figure 10 in Lok and Chan 2017). The correlation remains strong in all four simulated decades, suggesting the future seasonal variation of TC landfalls in South China can still be determined by the WNP subtropical ridge.

The influence of the El Niño-Southern Oscillation (ENSO) on TC activity throughout the projection is also examined (Table 2). While in the present-day climate simulation known relationships (e.g. Wang and Chan 2002; Goh and Chan 2010) can also be found, in the warmer climate the response of TC activity is less confined as correlation coefficients are generally smaller. It is also worthy to note that the

known ENSO-driven variability appears to be strengthened in the 2030s, while it is much weaker in the 2060s.

The different responses of TC activity to the ENSO may be due to differential variability in the large-scale environment. Figure 15 compares RegCM3 simulated 850-hPa large-scale circulation of the 2030s and 2060s under different ENSO condition. In the 2030s, the simulated low-level westerlies is governed by the ENSO-driven variation of the Walker circulation, with stronger westerlies in the WNP during El Niño years, and vice versa for La Niña years (Fig. 15a, c, e). In contrast, the simulated low-level circulation in the 2060s does not quite respond to the changing ENSO, the difference between the El Niño and La Niña years is much smaller (Fig. 15f) than that in the 2030s. From the detrended time series of the Niño3.4 calculated from HadGEM2-ES, more La Niña-like events are likely to occur around the middle of the twenty-first century. Liu and Chan (2017b) noted that variability in the Indian Ocean will also affect TC landfall in South China under La Niña condition. However, a preliminary investigation of our simulation results does not provide any indication of a

Fig. 14 Projected changes in **a**, **c**, **e** relative humidity at 850-hPa and **b**, **d**, **f** the magnitude of the vertical wind shear during the day of TC landfalls in South China from the present-day to **a**, **b** the 2030s, **c**, **d** the 2060s and **e**, **f** the 2090s. Significant negative changes at 95% confidence level are highlighted in light grey, whereas positive changes are marked in dark grey

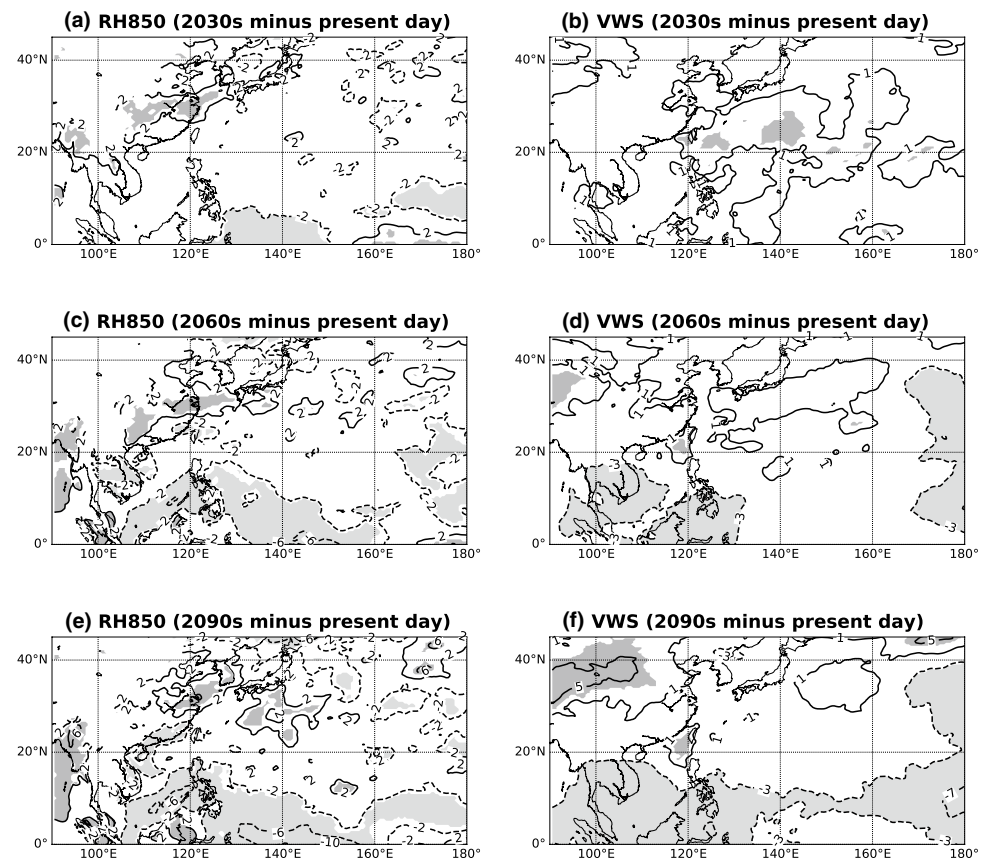


Table 2 Seasonal correlation coefficients between simulated TC variables and Niño 3.4 sea surface temperature index calculated from HadGEM2-ES over the four simulated decades

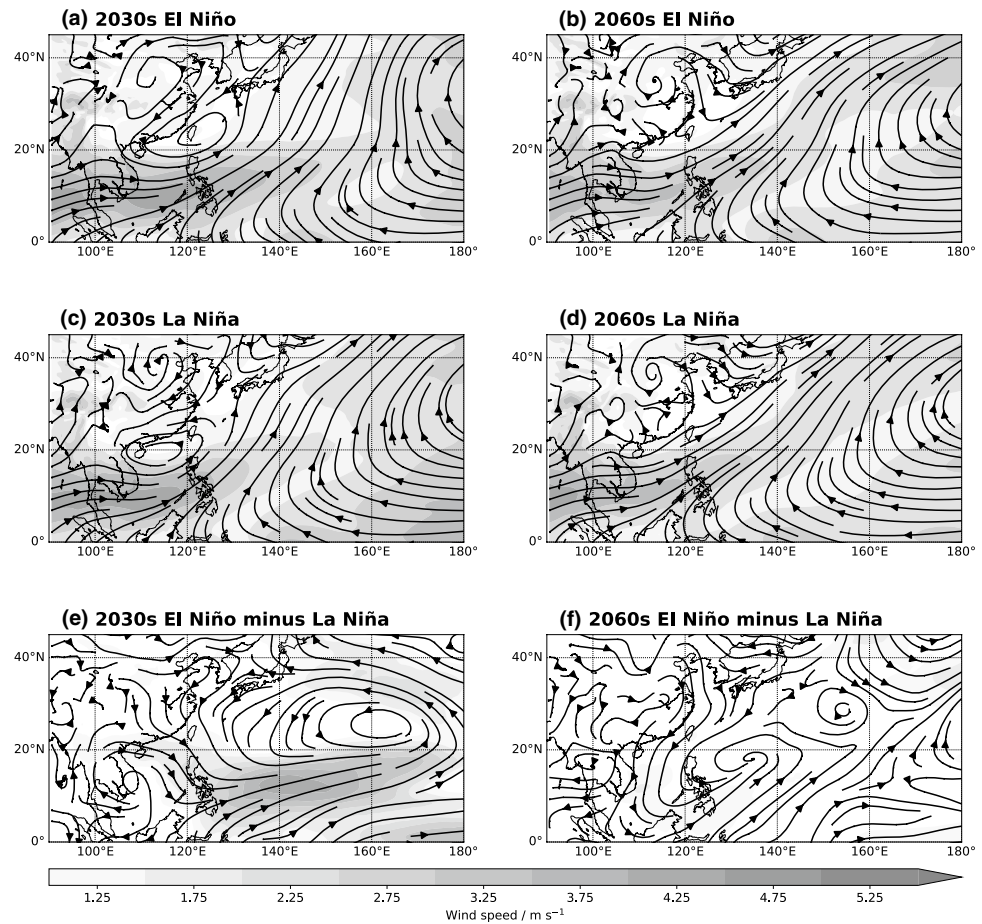
Variables	1996–2005	2030s	2060s	2090s
Mean genesis longitude	0.55	0.55	0.74	0.19
Mean genesis latitude	0.56	0.28	0.67	0.25
Number of TCs	-0.11	-0.32	0.14	-0.09
Number of landfalls in South China	-0.25	-0.81	-0.26	-0.34
APDI of South China	-0.21	-0.80	-0.07	-0.21

The Niño 3.4 index is the mean June–October SST anomaly of the area 5°N to 5°S and 170°W to 120°W. Boldface (italics) indicates 95% (90%) confidence correlation

relationship. Since there is larger uncertainty in the future response to the ENSO event, further research is needed before drawing any conclusion.

It should be noted that the above findings are based on one of the CMIP5 model only, and the model exhibits significant biases in reproducing the current climate. Multi-model ensemble simulations should be carried out for better future projections. Nevertheless the results in general are consistent with some previous studies (e.g. Knutson et al. 2015; Zhang et al. 2017). In particular, a recent study by Wang et al. (2017) also performed dynamical downscaling simulation from the same HadGEM2-ES model for TCs in the South China Sea. They also reported a decrease in TC frequency near the South China coast during the summertime, as well as an increase in the number of intense TCs. Both Wang et al. (2017) and this study projected similar changes in the environment as well. The agreement between two studies demonstrates that such a dynamical downscaling approach is useful and the results here can serve as a benchmark for future investigations.

Fig. 15 Composites of RegCM3 850-hPa wind fields for **a, b** El Niño, **c, d** La Niña years in the decades of **a, c** 2030 and **b, d** 2060. Wind speeds are shaded. Differences between El Niño and La Niña years in **e** the 2030s and **f** the 2060s. Significant differences in the wind fields are shaded



Acknowledgements We would like to thank Dr. Ralf Toumi and an anonymous reviewer for their constructive comments on this manuscript. This paper is part of the PhD project of the first author, and the study is supported by a Research Studentship from the City University of Hong Kong and Research Grants Council General Research Fund (Grant numbers CityU 100113 and E-CityU101/16). We acknowledge the World Climate Research Programme's Working Group on Coupled Modelling, which is responsible for CMIP, and we thank the Met Office Hadley Centre for producing and making available the HadGEM2-ES model output. For CMIP the U.S. Department of Energy's Program for Climate Model Diagnosis and Intercomparison provides coordinating support and led development of software infrastructure in partnership with the Global Organization for Earth System Science Portals.

Compliance with ethical standards

Conflict of interest The authors declare that they have no conflict of interest.

References

- Au-Yeung AYM, Chan JCL (2012) Potential use of a regional climate model in seasonal tropical cyclone activity predictions in the western North Pacific. *Clim Dyn* 39(3–4):783–794. <https://doi.org/10.1007/s00382-011-1268-x>
- Bister M, Emanuel KA (1998) Dissipative heating and hurricane intensity. *Meteorol Atmos Phys* 65(3):233–240. <https://doi.org/10.1007/BF01030791>
- Bister M, Emanuel KA (2002) Low frequency variability of tropical cyclone potential intensity 1. interannual to interdecadal variability. *J Geophys Res* 107(D24):4801. <https://doi.org/10.1029/2001JD000776>
- Black ML, Gamache JF, Marks FD, Samsbury CE, Willoughby HE (2002) Eastern Pacific Hurricanes Jimena of 1991 and Olivia of 1994: the effect of vertical shear on structure and intensity. *Mon Weather Rev* 130(9):2291–2312. [https://doi.org/10.1175/1520-0493\(2002\)130<2291:EPHJOA>2.0.CO;2](https://doi.org/10.1175/1520-0493(2002)130<2291:EPHJOA>2.0.CO;2)
- Camargo SJ (2013) Global and regional aspects of tropical cyclone activity in the CMIP5 models. *J Clim* 26(24):9880–9902. <https://doi.org/10.1175/JCLI-D-12-00549.1>
- Camargo SJ, Emanuel KA, Sobel AH (2007) Use of a genesis potential index to diagnose ENSO effects on tropical cyclone genesis. *J Clim* 20(19):4819–4834. <https://doi.org/10.1175/JCLI4282.1>
- Chan JCL (2006) Comment on changes in tropical cyclone number, duration, and intensity in a warming environment. *Science* 311(5768):1713. <https://doi.org/10.1126/science.1121522>
- Chan JCL, Xu M (2009) Inter-annual and inter-decadal variations of landfalling tropical cyclones in East Asia. Part I: time series analysis. *Int J Climatol* 29(9):1285–1293. <https://doi.org/10.1002/joc.1782>

- Chen C, Cane MA, Wittenberg AT, Chen D (2017a) ENSO in the CMIP5 simulations: life cycles, diversity, and responses to climate change. *J Clim* 30(2):775–801. <https://doi.org/10.1175/JCLI-D-15-0901.1>
- Chen TC, Tsay JD, Matsumoto J, Alpert J (2017b) Impact of the summer monsoon westerlies on the South China Sea tropical cyclone genesis in May. *Weather Forecast* 32(3):925–947. <https://doi.org/10.1175/WAF-D-16-0189.1>
- Chow KC, Chan JCL, Pal JS, Giorgi F (2006) Convection suppression criteria applied to the MIT cumulus parameterization scheme for simulating the Asian summer monsoon. *Geophys Res Lett* 33(24):L24,709. <https://doi.org/10.1029/2006GL028026>
- Chu JH, Sampson CR, Levine AS, Edward F (2002) The Joint Typhoon Warning Center tropical cyclone best-tracks, 1945–2000. Report, Joint Typhoon Warning Center, Pearl Harbor (United States). http://www.usno.navy.mil/NOOC/nmfc-ph/RSS/jtwc/best_tracks/TC_bt_report.html. Accessed 1 Sep 2017
- Collins WJ, Bellouin N, Doutriaux-Boucher M, Gedney N, Halloran P, Hinton T, Hughes J, Jones CD, Joshi M, Liddicoat S, Martin G, O'Connor F, Rae J, Senior C, Sitch S, Totterdell I, Wiltshire A, Woodward S (2011) Development and evaluation of an Earth-System model—HadGEM2. *Geosci Model Dev* 4(4):1051–1075. <https://doi.org/10.5194/gmd-4-1051-2011>
- Dickinson RE, A AS, Kennedy PJ, Wilson MF (1986) Biosphere-atmosphere transfer scheme (BATS) for the NCAR Community Climate Model. Technical Note TN-275+STR, National Center for Atmospheric Research, Boulder, Colorado (United States). <https://opensky.ucar.edu/islandora/object/technotes:383/datasream/PDF/view>. Accessed 1 Sep 2017
- Emanuel K (2005) Increasing destructiveness of tropical cyclones over the past 30 years. *Nature* 436(7051):686–688. <https://doi.org/10.1038/nature03906>
- Emanuel K, DesAutels C, Holloway C, Korty R (2004) Environmental control of tropical cyclone intensity. *J Atmos Sci* 61(7):843–858. [https://doi.org/10.1175/1520-0469\(2004\)061<0843:ECOTCI>2.0.CO;2](https://doi.org/10.1175/1520-0469(2004)061<0843:ECOTCI>2.0.CO;2)
- Emanuel KA (1986) An air-sea interaction theory for tropical cyclones. Part I: Steady-state maintenance. *J Atmos Sci* 43(6):585–605. [https://doi.org/10.1175/1520-0469\(1986\)043<0585:AASITF>2.0.CO;2](https://doi.org/10.1175/1520-0469(1986)043<0585:AASITF>2.0.CO;2)
- Emanuel KA (1999) Thermodynamic control of hurricane intensity. *Nature* 401(6754):665–669. <https://doi.org/10.1038/44326>
- Emanuel KA (2013) Downscaling CMIP5 climate models shows increased tropical cyclone activity over the 21st century. *Proc Natl Acad Sci USA* 110(30):12,219–12,224. <https://doi.org/10.1073/pnas.1301293110>
- Emanuel KA, Nolan DS (2004) Tropical cyclone activity and the global climate system. In: 26th Conference on Hurricanes and Tropical Meteorology, American Meteorological Society, Miami (United States)
- Emanuel KA, Živković Rothman M (1999) Development and evaluation of a convection scheme for use in climate models. *J Atmos Sci* 56(11):1766–1782. [https://doi.org/10.1175/1520-0469\(1999\)056<1766:DAEOAC>2.0.CO;2](https://doi.org/10.1175/1520-0469(1999)056<1766:DAEOAC>2.0.CO;2)
- Ferrier BS, Jin Y, Lin Y, Black T, Rogers E, DiMego G (2002) Implementation of a new grid-scale cloud and precipitation scheme in the NCEP Eta Model. In: 19th conference on weather analysis and forecasting/15th conference on numerical weather prediction, American Meteorological Society, San Antonio (United States)
- Goh AZC, Chan JCL (2010) Interannual and interdecadal variations of tropical cyclone activity in the south China sea. *Int J Climatol* 30(6):827–843. <https://doi.org/10.1002/joc.1943>
- Holland G, Bruyère CL (2014) Recent intense hurricane response to global climate change. *Clim Dyn* 42(3):617–627. <https://doi.org/10.1007/s00382-013-1713-0>
- Holtslag AAM, de Bruijn EIF, Pan HL (1990) A high resolution air mass transformation model for short-range weather forecasting. *Mon Weather Rev* 118(8):1561–1575. [https://doi.org/10.1175/1520-0493\(1990\)118<1561:AHRAWT>2.0.CO;2](https://doi.org/10.1175/1520-0493(1990)118<1561:AHRAWT>2.0.CO;2)
- Hong SY, Noh Y, Dudhia J (2006) A new vertical diffusion package with an explicit treatment of entrainment processes. *Mon Weather Rev* 134(9):2318–2341. <https://doi.org/10.1175/MWR3199.1>
- Huang WR, Chan JCL (2014) Dynamical downscaling forecasts of western North Pacific tropical cyclone genesis and landfall. *Clim Dyn* 42(7):2227–2237. <https://doi.org/10.1007/s00382-013-1747-3>
- Kain JS (2004) The Kain–Fritsch convective parameterization: an update. *J Appl Meteorol* 43(1):170–181. [https://doi.org/10.1175/1520-0450\(2004\)043<0170:TKCPAU>2.0.CO;2](https://doi.org/10.1175/1520-0450(2004)043<0170:TKCPAU>2.0.CO;2)
- Kerns BW, Chen SS (2013) Cloud clusters and tropical cyclogenesis: developing and nondeveloping systems and their large-scale environment. *Mon Weather Rev* 141(1):192–210. <https://doi.org/10.1175/MWR-D-11-00239.1>
- Kiehl JT, Hack JJ, Bonan GB, Boville BA, Briegleb BP, Williamson DL, Rasch PJ (1996) Description of the NCAR Community Climate Model (CCM3). Technical Note TN-420+STR, National Center for Atmospheric Research, Boulder, Colorado (United States). <https://opensky.ucar.edu/islandora/object/technotes:187/datasream/PDF/view>. Accessed 1 Sep 2017
- Klotzbach PJ, Landsea CW (2005) Extremely intense hurricanes: revisiting Webster et al. (2005) after 10 years. *J Clim* 28(19):7621–7629. <https://doi.org/10.1175/JCLI-D-15-0188.1>
- Knutson TR, McBride JL, Chan JCL, Emanuel KA, Holland GJ, Landsea C, Held IM, Kossin JP, Srivastava AK, Sugi M (2010) Tropical cyclones and climate change. *Nat Geosci* 3(3):157–163. <https://doi.org/10.1038/ngeo779>
- Knutson TR, Sirutis JJ, Vecchi GA, Garner S, Zhao M, Kim HS, Bender M, Tuleya RE, Held IM, Villarini G (2013) Dynamical downscaling projections of twenty-first-century Atlantic hurricane activity: CMIP3 and CMIP5 model-based scenarios. *J Clim* 26(17):6591–6617. <https://doi.org/10.1175/JCLI-D-12-00539.1>
- Knutson TR, Sirutis JJ, Zhao M, Tuleya RE, Bender M, Vecchi GA, Villarini G, Chavas D (2015) Global projections of intense tropical cyclone activity for the late twenty-first century from dynamical downscaling of CMIP5/RCP4.5 scenarios. *J Clim* 28(18):7203–7224. <https://doi.org/10.1175/JCLI-D-15-0129.1>
- Liang J, Wang C, Hodges KI (2017) Evaluation of tropical cyclones over the South China Sea simulated by the 12 km MetUM regional climate model. *Q J R Meteorol Soc* 143(704):1641–1656. <https://doi.org/10.1002/qj.3035>
- Liu KS, Chan JCL (2017a) Variations in the power dissipation index in the East Asia region. *Clim Dyn* 48(5):1963–1985. <https://doi.org/10.1007/s00382-016-3185-5>
- Liu KS, Chan JCL (2017b) Changing relationship between La Niña and tropical cyclone landfalling activity in South China (La Niña and TC landfalling activity in South China). *Int J Climatol Adv*. <https://doi.org/10.1002/joc.5242>
- Lok CCF, Chan JCL (2017) Simulating seasonal tropical cyclone intensities at landfall along the South China coast. *Clim Dyn* Adv. <https://doi.org/10.1007/s00382-017-3762-2>
- McBride JL, Zehr R (1981) Observational analysis of tropical cyclone formation. Part II: Comparison of non-developing versus developing systems. *J Atmos Sci* 38(6):1132–1151. [https://doi.org/10.1175/1520-0469\(1981\)038<1132:OAOTCF>2.0.CO;2](https://doi.org/10.1175/1520-0469(1981)038<1132:OAOTCF>2.0.CO;2)
- McSweeney CF, Jones RG, Lee RW, Rowell DP (2015) Selecting CMIP5 GCMs for downscaling over multiple regions. *Clim Dyn* 44(11):3237–3260. <https://doi.org/10.1007/s00382-014-2418-8>
- Mlawer EJ, Taubman SJ, Brown PD, Iacono MJ, Clough SA (1997) Radiative transfer for inhomogeneous atmospheres: RRTM, a

- validated correlated-k model for the longwave. *J Geophys Res* 102(D14):16,663–16,682. <https://doi.org/10.1029/97JD00237>
- Monin A, Obukhov A (1954) Basic laws of turbulent mixing in the surface layer of the atmosphere. Trudy Geofizicheskogo Instituta Akademii Nauk SSSR 24(151):163–187
- Murakami H, Wang B (2010) Future change of north Atlantic tropical cyclone tracks: projection by a 20-km-mesh global atmospheric model. *J Clim* 23(10):2699–2721. <https://doi.org/10.1175/2010JCLI3338.1>
- Pal JS, Small EE, Eltahir EAB (2000) Simulation of regional-scale water and energy budgets: representation of subgrid cloud and precipitation processes within RegCM. *J Geophys Res* 105(D24):29,579–29,594. <https://doi.org/10.1029/2000JD900415>
- Pal JS, Giorgi F, Bi X, Elguindi N, Solmon F, Rauscher SA, Gao X, Francisco R, Zakey A, Winter J, Ashfaq M, Syed FS, Sloan LC, Bell JL, Difffenbaugh NS, Karmacharya J, Konaré A, Martinez D, da Rocha RP, Steiner AL (2007) Regional climate modeling for the developing world: the ICTP RegCM3 and RegCNET. *Bull Am Meteorol Soc* 88(9):1395–1409. <https://doi.org/10.1175/BAMS-88-9-1395>
- Park DSR, Ho CH, Chan JCL, Ha KJ, Kim HS, Kim J, Kim JH (2017) Asymmetric response of tropical cyclone activity to global warming over the North Atlantic and western North Pacific from CMIP5 model projections. *Sci Rep* 7(41):354. <https://doi.org/10.1038/srep41354>
- Saha S, Moorthi S, Pan HL, Wu X, Wang J, Nadiga S, Tripp P, Kistler R, Woollen J, Behringer D, Liu H, Stokes D, Grumbine R, Gayno G, Wang J, Hou YT, Chuang HY, Juang HMH, Sela J, Iredell M, Treadon R, Kleist D, van Delst P, Keyser D, Derber J, Ek M, Meng J, Wei H, Yang R, Lord S, van den Dool H, Kumar A, Wang W, Long C, Chelliah M, Xue Y, Huang B, Schemm JK, Ebisuzaki W, Lin R, Xie P, Chen M, Zhou S, Higgins W, Zou CZ, Liu Q, Chen Y, Han Y, Cucurull L, Reynolds RW, Rutledge G, Goldberg M (2010) The NCEP climate forecast system reanalysis. *Bull Am Meteorol Soc* 91(8):1015–1057. <https://doi.org/10.1175/2010BAMS3001.1>
- Shay LK, Goni GJ, Black PG (2000) Effects of a warm oceanic feature on Hurricane Opal. *Mon Weather Rev* 128(5):1366–1383. [https://doi.org/10.1175/1520-0493\(2000\)128<1366:EOAWOF>2.0.CO;2](https://doi.org/10.1175/1520-0493(2000)128<1366:EOAWOF>2.0.CO;2)
- Taylor KE, Stouffer RJ, Meehl GA (2012) An overview of CMIP5 and the experiment design. *Bull Am Meteorol Soc* 93(4):485–498. <https://doi.org/10.1175/BAMS-D-11-00094.1>
- Tory KJ, Chand SS, McBride JL, Ye H, Dare RA (2013) Projected changes in late-twenty-first-century tropical cyclone frequency in 13 coupled climate models from phase 5 of the coupled model intercomparison project. *J Clim* 26(24):9946–9959. <https://doi.org/10.1175/JCLI-D-13-00010.1>
- Tory KJ, Chand SS, McBride JL, Ye H, Dare RA (2014) Projected changes in late 21st century tropical cyclone frequency in CMIP5 models. In: 31th Conference on Hurricanes and Tropical Meteorology, American Meteorological Society, San Diego (United States). <https://ams.confex.com/ams/31Hurr/webprogram/Paper245100.html>. Accessed 1 Sep 2017
- Villarini G, Vecchi GA (2012) Twenty-first-century projections of North Atlantic tropical storms from CMIP5 models. *Nat Clim Change* 2(8):604–607. <https://doi.org/10.1038/nclimate1530>
- Wang B, Chan JCL (2002) How strong ENSO events affect tropical storm activity over the western North Pacific. *J Clim* 15(13):1643–1658. [https://doi.org/10.1175/1520-0442\(2002\)015<1643:HSEEAT>2.0.CO;2](https://doi.org/10.1175/1520-0442(2002)015<1643:HSEEAT>2.0.CO;2)
- Wang C, Liang J, Hodges KI (2017) Projections of tropical cyclones affecting Vietnam under climate change: downscaled HadGEM2-ES using PRECIS 2.1. *Q J R Meteorol Soc* 143(705):1844–1859. <https://doi.org/10.1002/qj.3046>
- Webster PJ, Holland GJ, Curry JA, Chang HR (2005) Changes in tropical cyclone number, duration, and intensity in a warming environment. *Science* 309(5742):1844–1846. <https://doi.org/10.1126/science.1116448>
- Ying M, Knutson TR, Kamahori H, Lee TC (2012) Impacts of climate change on tropical cyclones in the western North Pacific basin Part II: late twenty-first century projections. *Trop Cycl Res Rev* 1(2):231–241. <https://doi.org/10.6057/2012TCRR02.09>
- Yoshida R, Miyamoto Y, Tomita H, Kajikawa Y (2017) The effect of water vapor on tropical cyclone genesis: a numerical experiment of a non-developing disturbance observed in PALAU2010. *J Meteorol Soc Jpn* 95(1):35–47. <https://doi.org/10.2151/jmsj.2017-001>
- Yun KS, Yeh SW, Ha KJ (2016) Inter-El Niño variability in CMIP5 models: model deficiencies and future changes. *J Geophys Res* 121(8):3894–3906. <https://doi.org/10.1002/2016JD024964>
- Zhang L, Karnauskas KB, Donnelly JP, Emanuel K (2017) Response of the North Pacific tropical cyclone climatology to global warming: application of dynamical downscaling to CMIP5 models. *J Clim* 30(4):1233–1243. <https://doi.org/10.1175/JCLI-D-16-0496.1>